Supporting Information

Enhancing the separation efficiency of C_2H_2/C_2H_4 mixture by a chromium Metal-Organic Framework fabricated via post-synthetic metalation

Fan Yu[a],* Bing-Qian Hu,[a] Xiao-Ning Wang,[b] Yu-Meng Zhao,[b] Jia-Luo Li[c], Bao Li [b],* and Hong-Cai Zhou[c,]*

a. Key Laboratory of Optoelectronic Chemical Materials and Devices of Ministry of Education, School of Chemical and Environmental Engineering Jianghan University, Wuhan, 430056, PR China.

b. Key laboratory of Material Chemistry for Energy Conversion and Storage, School of Chemistry and Chemical Engineering, Huazhong University of Science and Technology, Wuhan, Hubei, 430074, PR China.

c. Department of Chemistry, Texas A&M University, College Station, Texas 77843-3255, United States.

*E-mails: yufan0714@163.com;libao@hust.edu.cn; zhou@chem.tamu.edu

Contents

Experimental Section

Materials and methods.

All starting chemicals were purchased from commercial sources and were used without further purification. The starting materials, tri-nuclear Fe_3O and hexa-carboxyl ligands, had been synthesized according to the references.[1,2]

Elemental analyses (C, H and N) were determined on a Perkin-Elmer 2400 analyzer. Thermogravimetric analysis (TGA) was performed on a Perkin-Elmer TG-7 analyzer heated from 25 to 800 ℃ under nitrogen atmosphere. Powder X-ray diffraction (PXRD) patterns for the as-synthesized samples were recorded on a X-ray diffraction meter (D/max 2500 PC, Rigaku) with Cu-*K*α radiation (1.5406 Å). N_2 adsorption−desorption isotherms were measured using a Micromeritics ASAP 2020 system at 77 K for all of the samples that have been immersed in acetone for three days and activated at 120 ℃ for 10h. The morphologies of the hierarchical derivatives were observed by using a SU8020 Scanning Electron Microscope (SEM, Hitachi, Japan). Energy dispersive X-ray spectra (EDS) of different elements in different samples was recorded via SEM. X-ray photoelectron spectroscopy (XPS) was carried out on a VGESCALBMKII X-ray photoelectron system with an Al *K*α radiation (1486.6 eV).

Syntheses of HUST-5

Solid Fe_3O material (0.038 g) and hexa-carboxyl ligand (0.040g) was added to 12 mL DMF and the solution was stirred for 5 min, and then added 3.2 ml acetate acid. The mixture was sealed in a 25 mL stainless steel reactor and heated to 150 °C within 3 days, and then cooled to 30 °C within 500 min. Red block crystals of HUST-5 were obtained by filtration. Yield: ~43% based on ligands. Elemental analysis calcd (%) for desolvent sample $C_{85}H_{57}Fe_6N_6O_{44}P_6$: C 42.76, H 2.41, N 3.52. Found: C 43.40, H 2.85, N 4.06.

Syntheses of HUST-6

100mg $CrCl_3 \cdot 6H_2O$ was dissolved in acetone 20 mL. Then 30mg solid crystal sample of HUST-5 had been immersed in 5 mL acetone solutions at 60℃. The solution had been changed after 24 h. After three days, green samples had been filtered and washed with acetone for three times.

Syntheses of HUST-5 with $FeCl_2$

$FeCl_2 \cdot 4H_2O$ (0.18 mmol, 36 mg) and H_6L (0.042 mmol, 40 mg) were ultrasonically dissolved in 12 mL DMF and 1 mL H_2O, and formic acid (1.6 mL) was then added to the solution in a 20 mL glass vial. The vial was then heated at 120 °C for 5 days in an oven. After cooling to room temperature, the red block crystals were harvested by filtration and washed with DMF. The yield was 48% for HUST-5 (based on H_6L ligand).

Pure gas adsorption

Gas sorption isotherms were performed on Micromeritics (3FLEX) aparatus. Prior to gas measurement, the dichloromethane-exchanged samples were degassed at 80^{o}C under dynamic vacuum for 48h.

Breakthrough tests

The breakthrough experiments were carried out in homemade dynamic gas breakthrough equipment. A stainless steel column (4.6 mm inner diameter × 50 mm) packed with 0.835 g activated **NbU-1** powder was firstly purged with He flow (5 ml min^{-1}) for 1 h at 293K. The mixed C_2H_2/C_2H_4 gas (50/50, v/v) flow was introduced at 2.0 ml min^{-1}, another mixed C_2H_2/C_2H_4 gas (1/99, v/v) flow was introduced at 1.0 ml min^{-1}. The relative amounts of the gases passing through the column were monitored using gas chromatography (Agilent 7890B) with a thermal conductivity detector (TCD) once every 30 seconds, after 180 minutes, the test becomes to once every 5 minutes. After every separation experiment, the adsorption bed was regenerated by heating at 50^{o}C under vacuum conditions for 2 hours. The transient breakthrough

simulation results are presented in terms of a dimensionless time, τ_{break}, defined by dividing the actual time, t, by the characteristic time, $L\varepsilon u^{-1}$(L: length of packed bed; ε:voidage of packed bed, u:superficial gas velocity at inlet).

IAST adsorption selectivity calculation:

The experimental isotherm data for pure C_2H_2, C_2H_4, C_2H_6, and CH_4 (measured at 273 K) were fitted using a Langmuir-Freundlich (L-F) model:

$$q = \frac{a * b * p^c}{1 + b * P^c}$$

Where q and p are adsorbed amounts and pressures of component i, respectively.

Using the pure component isotherm fits, the adsorption selectivity is defined by

$$S_{ads} = \frac{q_1 / q_2}{p_1 / p_2}$$

Where q_i is the amount of i adsorbed and p_i is the partial pressure of i in the mixture.

We used the following written codes to simulate the adsorption selectivity of C_2H_2/C_2H_4 in Fig. 6:

```
28                          # No. of Pressure Point
y1, y2                      # Molar fraction of binary mixture (y1 and y2, y1 + y2 = 1)
1, 2, 3, 4, 5, 6, 7, 8, 9, 10, 20, 30, 40, 50, 60, 70, 80, 90, 100, 101, 102, 103, 104, 105, 106, 107,
108, 109                    #The unit is same parameter b, kPa
a1, a2                      # fitting parameter Nsat (A1) for both component (Unit: mmol/g)
b1, b2                      # fitting parameter b1 for both components (Unit: kPa-1)
c1, c2                      # fitting parameter c1 for both components
0, 0                        # fitting parameter Nsat2(A2) for both component(Unit: mmol/g)
0, 0                        # fitting parameter b2 for both components (Unit: kPa-1)
1, 1                        # fitting parameter c2 for both components
```

X-Ray Structural Determination. Diffraction data for HUST-5 (0.1 × 0.05 × 0.05 mm) was collected via Bruker Venture using Cu-$K\alpha$ (λ = 1.54178 Å) radiation at 100

K. The structures of complexes were solved by direct methods, and the non-hydrogen atoms were located from the trial structure and then refined anisotropically with SHELXTL using a full-matrix leastsquares procedure based on F^2 values. The hydrogen atom positions were fixed geometrically at calculated distances and allowed to ride on the parent atoms. Attempts to define the highly disordered solvent molecules were unsuccessful, so the structure was refined with the PLATON "SQUEEZE" procedure. The diffraction intensity of crystal sample was very weak due to the very small size and low density, which must be responsible for the corresponding alert A. CCDC-1913173 for the data under different temperature contain the supplementary crystallographic data for this paper. These data can be obtained free of charge from The Cambridge Crystallographic Data Centre via http://www.ccdc.cam.ac.uk/datarequest/cif.

Computational Detail

Spin polarized Density functional theory calculations were performed by using DMol3 software in the Material Studio module[3]. Perdew–Burke–Ernzerhof (PBE) functional with generalized gradient approximation (GGA) [4] was used to describe exchange-correlation (XC) effects was treated by. All electron numerical basis set of double numerical plus polarization (DNP) [5] were used to expand electronic wave function. For Fe or Cr ions, the Effective Core Potentials (ECP) [6] replaces core electrons by a single effective potential, and valence electrons were described by DNP numerical basic set. DFT-D corrections with Grimme method [3] was used to the treatment of weak dispersion energy. In the optimization calculation, 2.0×10^{-5} Ha and 2.0×10^{-3} Ha. $Å^{-1}$ were set as the convergence value of energy and force, and the threshold for SCF density convergence was 1.0×10^{-6}. Hirshfeld charge population analysis and frontier molecular orbital analysis were further performed.

Owing to the restriction of huge computational cost and theoretical method, it is very different to perform the simulation toward the whole MOF framework. Inspecting the microscopic structure, $(M_3O)_2(H_2O)_4(HCOO)(L2)_4$ unit, dominating properties of MOFs, was regarded as computational model. The original hexa-carboxyl ligands L1 had been simplified as tetra-carboxy ligand as L2, labeled as

4,4',4",4"'-((6,6-dihydroxy-1,3,5,2l5,4l5,6l5-triazatriphosphinine-2,2,4,4-tetrayl) tetrakis(oxy))tetrabenzoic acid, scheme S1). The terminal atoms of the model were saturated by additional hydrogen atoms. Adsorption energy were typically calculated based following formula: $E_a(X) = E(X\text{- MOF}) - E(\text{MOF}) - E(X)$(X= C_2H_2, C_2H_4), where E(X- MOF), E(MOF) and E(X) were single-point energy of relaxed geometry of X-MOF, MOF and X with the same computational setting. Meanwhile, dissociation energy of aqua ligand was evaluated according to this formula: $E_d = E(H_2O) + E(\text{Cr-MOF-}H_2O) - E(\text{Cr-MOF})$, where E(Cr-MOF), E(Cr-MOF-H_2O) and E(H_2O) were single-point energy of relaxed structure of original Cr-MOF, H_2O-removed Cr-MOF and H_2O with the same computational setting.

Table S1 Crystal data of HUST-5

Empirical formula	$C_{85}H_{57}Fe_6N_6O_{44}P_6$
Formula weight	2387.29
Crystal system	monoclinic
Space group	*C*2
a/Å	27.9272(17)
b/Å	20.8710(17)
c/Å	35.446(3)
α/°	90
β/°	93.965(6)
γ/°	90
Volume/Å^3	20611(3)
Z	4
ρ_{calc}g/cm^3	0.769
μ/mm^{-1}	4.141
F(000)	10272.0
Goodness-of-fit on F^2	1.047
Final R indexes [I>=2σ (I)]	R_1 = 0.1025, wR_2 = 0.2501
Final R indexes [all data]	R_1 = 0.1379, wR_2 = 0.2706
Largest diff. peak/hole / e Å^{-3}	0.66/-0.61
Flack parameter	0.271(6)

Table S2 Selected Bond Lengths for HUST-5

Atom	Atom	Length/Å	Atom	Atom	Length/Å
Fe1	O2	2.060(9)	O21	Fe6	2.082(9)
Fe1	O41	1.969(10)	O40	Fe3	2.066(12)
Fe1	O24	1.971(9)	O20	Fe5	1.945(10)
Fe1	O4	1.965(10)	O28	Fe5[3]	1.990(9)
Fe1	O38	1.978(9)	O26	Fe6[3]	2.025(9)
Fe1	O7[1]	2.040(11)	C60	C59	1.439(11)
O11	Fe4[2]	2.030(8)	O42	Fe6	2.080(13)
O8	Fe2[2]	1.976(10)	O30	Fe6[4]	1.936(10)
O44	Fe5	1.891(11)	O12	Fe6[2]	1.977(9)
O44	Fe4	1.919(9)	O23	Fe3	1.984(9)
O44	Fe6	1.935(9)	O3	Fe3	1.934(10)
O41	Fe2	1.944(10)	O9	Fe3[2]	2.037(9)
O41	Fe3	1.849(10)	O6	Fe3[5]	2.010(11)
O10	Fe2[2]	1.968(10)	Fe2	O8[1]	1.976(10)
O27	Fe4[3]	1.991(8)	Fe2	O10[1]	1.968(10)
O22	Fe5	2.008(10)	Fe2	O5[5]	2.036(10)
O19	Fe4	2.008(10)	Fe3	O9[1]	2.037(9)
O1	Fe2	1.960(9)	Fe3	O6[5]	2.010(11)
O29	Fe5[4]	2.043(10)	Fe5	O29[6]	2.043(10)
O25	Fe4[3]	2.051(12)	Fe5	O28[7]	1.990(9)
O43	Fe5	2.061(10)	Fe4	O11[1]	2.030(8)
O5	Fe2[5]	2.036(10)	Fe4	O27[7]	1.991(8)
Fe6	O30[6]	1.936(10)	Fe4	O25[7]	2.051(12)
Fe6	O12[1]	1.977(9)	Fe6	O26[7]	2.025(9)
O7	Fe1[2]	2.040(11)			

Asymmetric colde : [1]-1/2+X,1/2+Y,+Z; [2]1/2+X,-1/2+Y,+Z; [3]-1/2+X,-1/2+Y,+Z; [4]5/2-X,-1/2+Y,-Z; [5]3-X,+Y,-1-Z; [6]5/2-X,1/2+Y,-Z; [7]1/2+X,1/2+Y,+Z

Table S3. ICP-MS results of sectional metal metathesis

	HUST-5	HUST-6
Cr (μg L^{-1})	0	259.28
Fe (μg L^{-1})	356.37	2.07
Cr/Fe ratio (%)	0	125.26

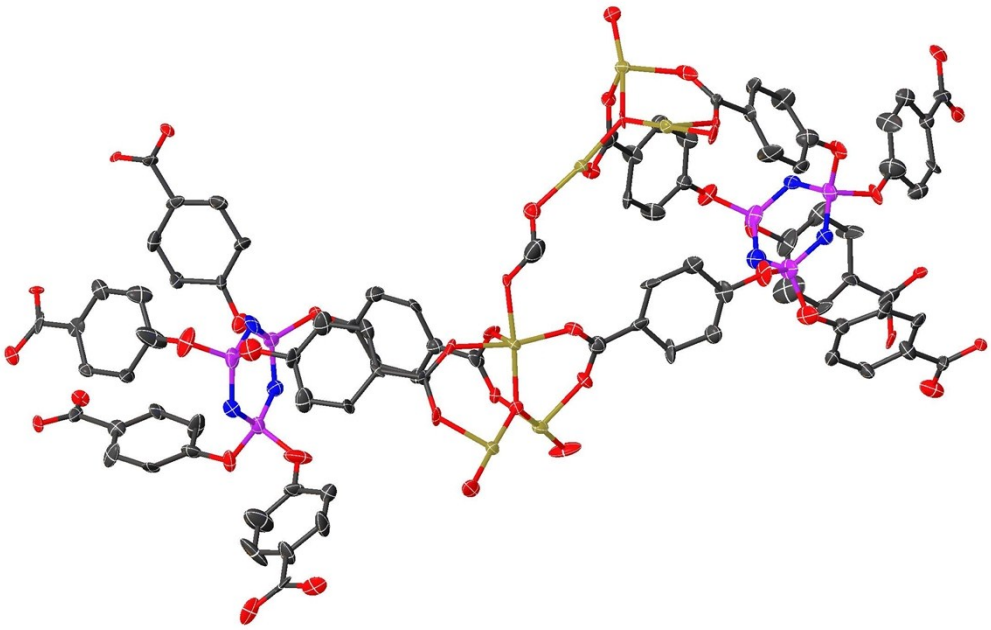

Figure S1. The asymmetric unit of HUST-5

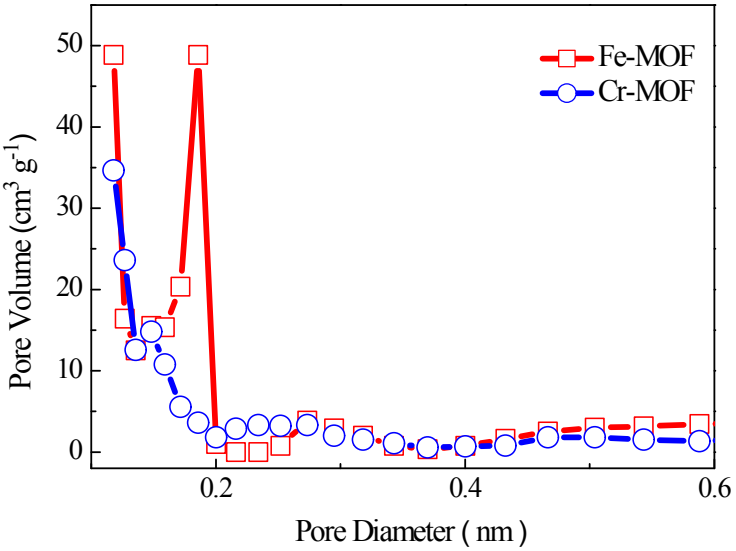

Figure S2. Pore size distribution curves obtained by the Horvath–Kawazoe method for HUST-5 and HUST-6.

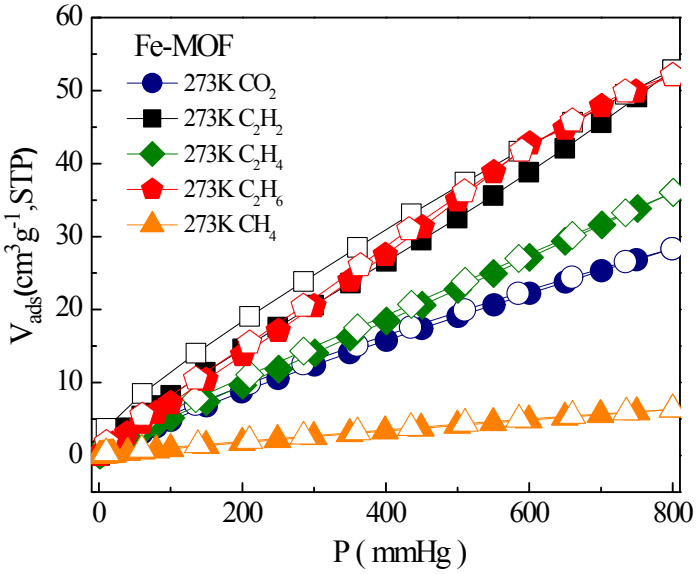

Figure S3. Enlarged CO_2 , CH_4 and C_2H_x sorption isotherms for HUST-5

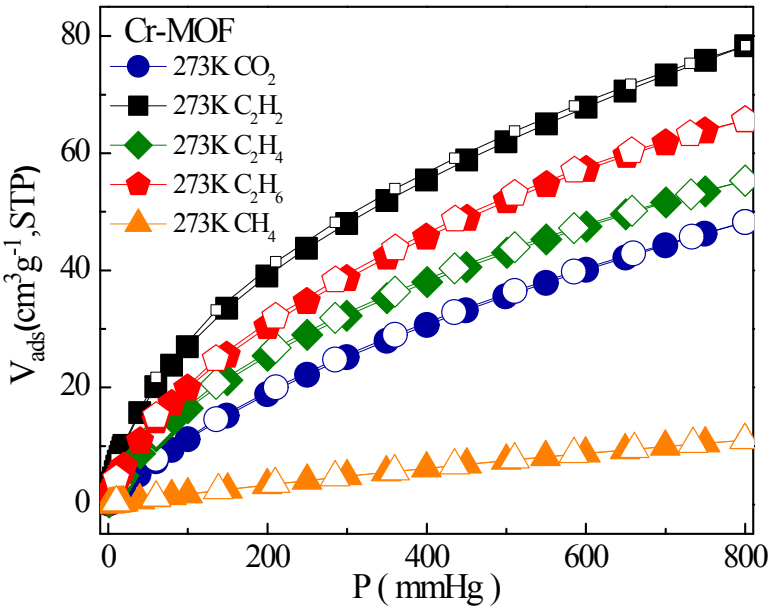

Figure S4. Enlarged CO_2 , CH_4 and C_2H_x sorption isotherms for HUST-6

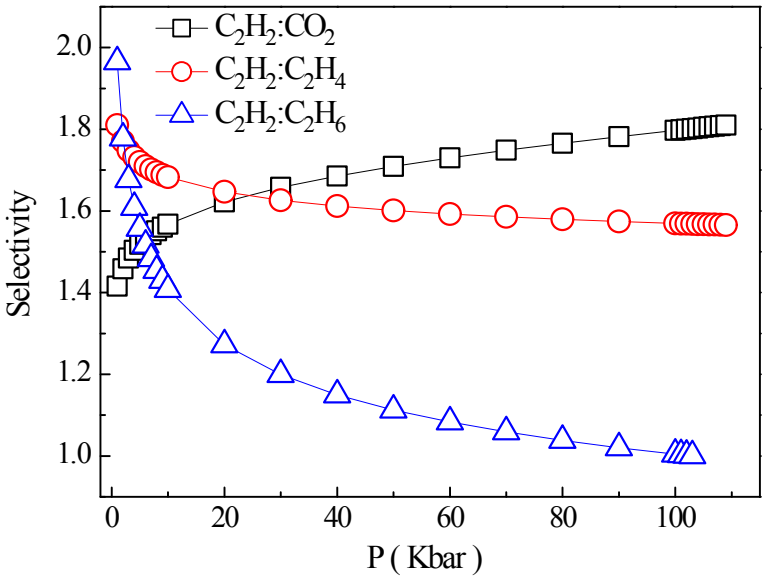

Figure S5. Enlarged IAST adsorption selectivities for HUST-5 of equimolar C_2H_2/C_2H_x and C_2H_2/CO_2 mixtures

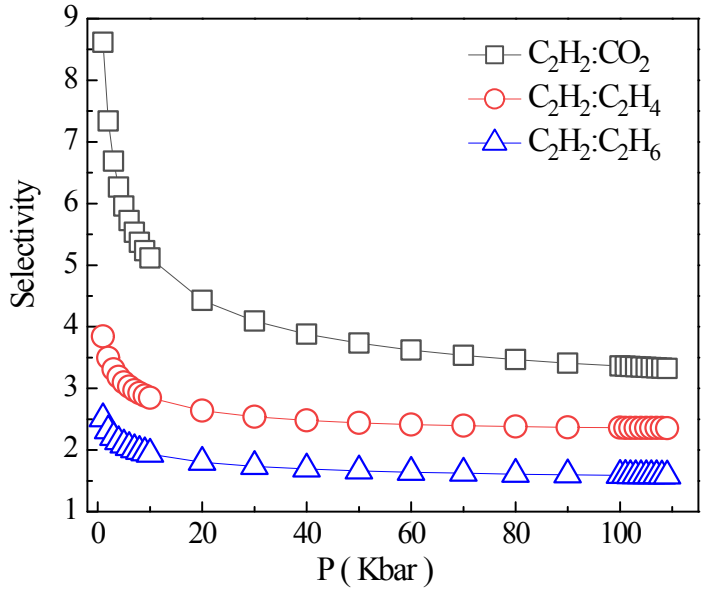

Figure S6. Enlarged IAST adsorption selectivities for HUST-6 of equimolar C_2H_2/C_2H_x and C_2H_2/CO_2 mixtures

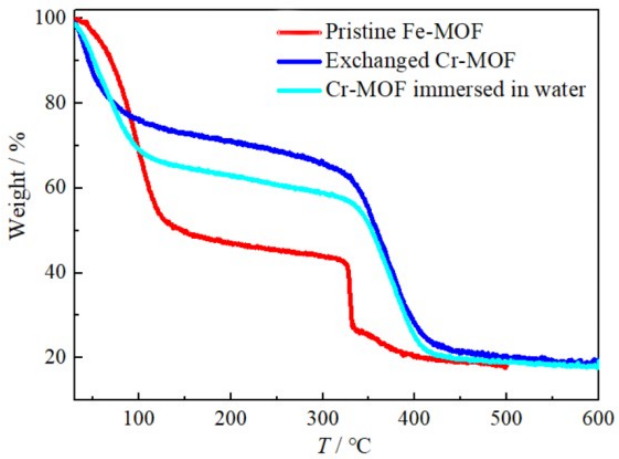

Figure S7. TGA curves of pristine HUST-5, as-synthesized HUST-6 and HUST-6 immersed in water.

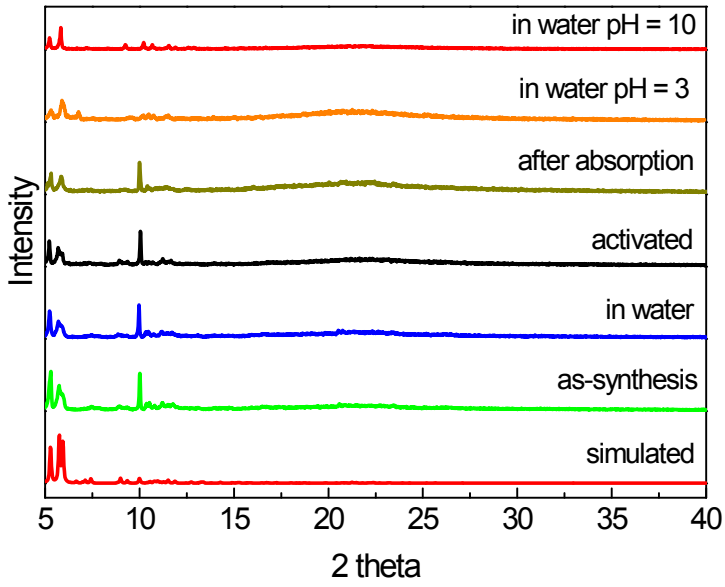

Figure S8. XRD pattern of HUST-5 under different conditions

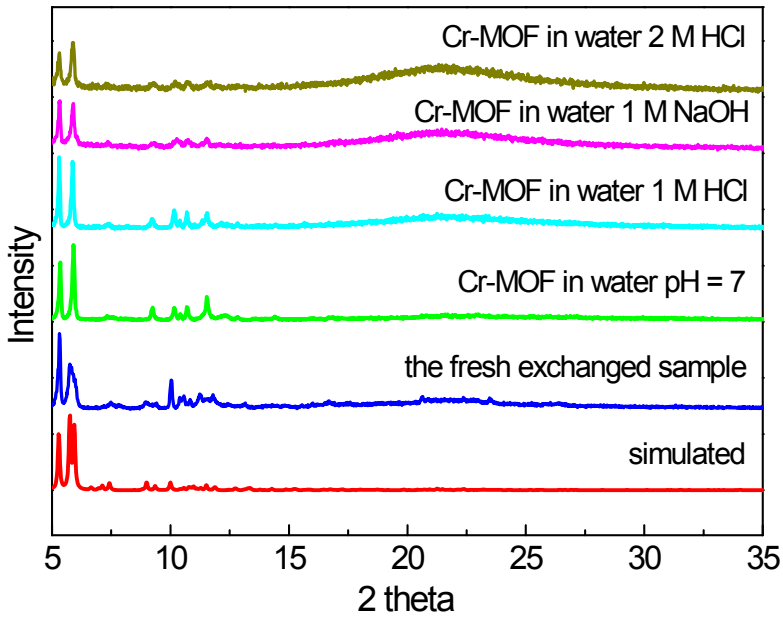

Figure S9. XRD pattern of HUST-6 under different conditions

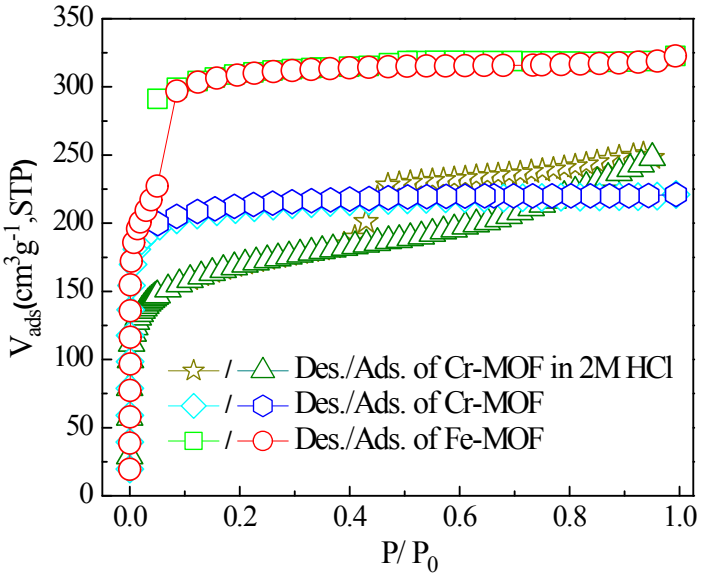

Figure S10. N_2 sorption isotherms for activated HUST-5, HUST-6 and HUST-6 immersed in 2M HCl at 77K after vacuum-drying at 150 °C overnight.

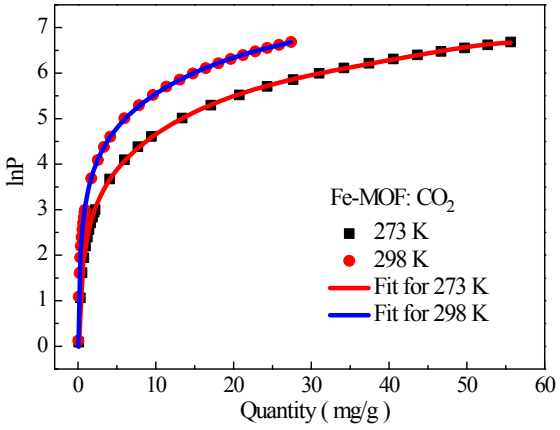

Model	Qst (User)		
Equation	y=ln(x)+1/K*(a0+a1*x+a2*x^2+a3*x^3+a4*x^4+a5*x^5)+(b0+b1*x+ b2*x^2)		
Reduced Chi-Sqr			0.00122
Adj. R-Square			0.99968
		Value	Standard Err
Quantity	a0*	-3048.3223	52.83444
	a1*	10.89235	13.569
	a2*	0.65262	0.60052
	a3*	-0.03515	0.01383
	a4*	7.02778E-	2.92358E-4
	a5*	-4.90081E-	2.17981E-6
	b0*	13.39704	0.18313
	b1*	-0.04203	0.04604
	b2*	7.00972E-	0.00175
	K	273	0
ln P	a0*	-3048.3223	52.83444
	a1*	10.89235	13.569
	a2*	0.65262	0.60052
	a3*	-0.03515	0.01383
	a4*	7.02778E-	2.92358E-4
	a5*	-4.90081E-	2.17981E-6
	b0*	13.39704	0.18313
	b1*	-0.04203	0.04604
	b2*	7.00972E-	0.00175
	K	298	0

Fig. S11 The CO_2 fit isotherms of **HUST-5** at 273 K and 298 K by virial equation.

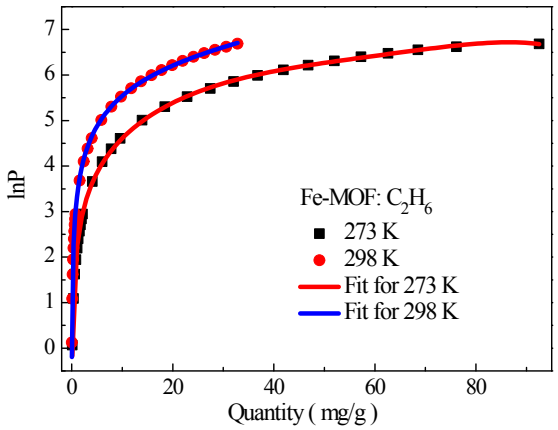

Model	Qst (User)		
Equation	y=ln(x)+1/K*(a0+a1*x+a2*x^2+a3*x^3 +a4*x^4+a5*x^5)+(b0+b1*x+ b2*x^2)		
Reduced Chi-Sqr			0.00476
Adj. R-Square			0.99876
		Value	Standard Err
Quantity	a0*	-3682.2072	104.11877
	a1*	78.69593	22.48095
	a2*	-1.33501	0.81228
	a3*	-0.00416	0.00727
	a4*	7.32183E-	9.43488E-5
--	a5*	-3.78602E-	4.28742E-7
	b0*	15.66489	0.3612
	b1*	-0.27455	0.07554
	b2*	0.00495	0.00243
	K	273	0
ln P	a0*	-3682.2072	104.11877
	a1*	78.69593	22.48095
	a2*	-1.33501	0.81228
	a3*	-0.00416	0.00727
	a4*	7.32183E-	9.43488E-5
--	a5*	-3.78602E-	4.28742E-7
	b0*	15.66489	0.3612
	b1*	-0.27455	0.07554
	b2*	0.00495	0.00243
	K	298	0

Fig. S12 The C_2H_6 fit isotherms of **HUST-5** at 273 K and 298 K by virial equation.

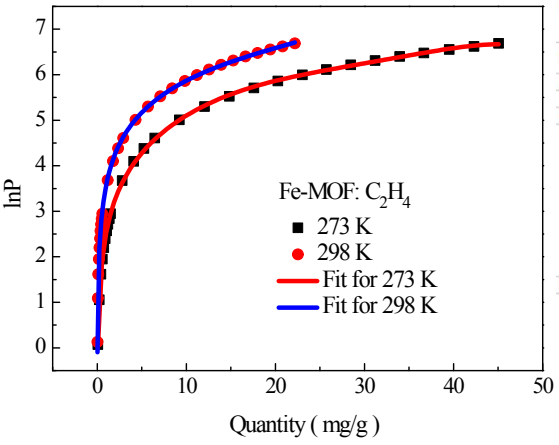

Model	Qst (User)		
Equation	y=ln(x)+1/K*(a0+a1*x+a2*x^2+a3*x^3 +a4*x^4+a5*x^5)+(b0+b1*x+ b2*x^2)		
Reduced Chi-Sqr			0.00236
Adj. R-Square			0.99938
		Value	Standard Err
Quantity	a0*	-3515.4071	73.98873
	a1*	143.61116	23.27525
	a2*	-3.92376	1.27809
	a3*	-0.03642	0.03621
	a4*	0.00122	9.49597E-4
--	a5*	-1.2115E-5	8.77302E-6
	b0*	15.36596	0.25671
	b1*	-0.48938	0.07897
	b2*	0.01472	0.00374
	K	273	0
ln P	a0*	-3515.4071	73.98873
	a1*	143.61116	23.27525
	a2*	-3.92376	1.27809
	a3*	-0.03642	0.03621
	a4*	0.00122	9.49597E-4
--	a5*	-1.2115E-5	8.77302E-6
	b0*	15.36596	0.25671
	b1*	-0.48938	0.07897
	b2*	0.01472	0.00374
	K	298	0

Fig. S13 The C_2H_4 fit isotherms of **HUST-5** at 273 K and 298 K by virial equation.

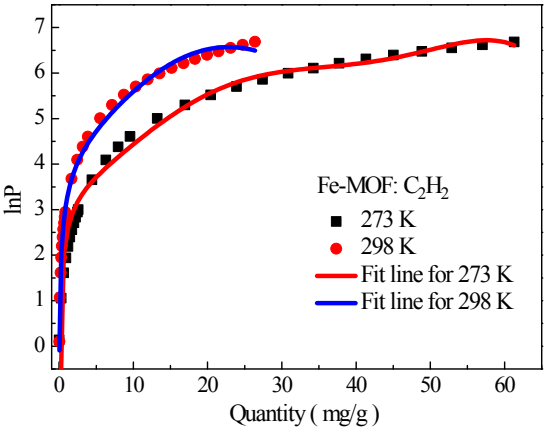

Model	Qst (User)		
Equation	y=ln(x)+1/K*(a0+a1*x+a2*x^2+a3*x^3 +a4*x^4+a5*x^5)+(b0+b1*x+ b2*x^2)		
Reduced Chi-Sqr			0.15723
Adj. R-Square			0.95853
		Value	Standard Err
Quantity	a0*	-2159.8567	629.62864
	a1*	-294.99601	162.47123
	a2*	15.22036	7.34837
	a3*	-0.22164	0.12131
	a4*	0.00374	0.00232
--	a5*	-2.27363E-	1.56546E-5
	b0*	10.50414	2.17915
	b1*	0.89928	0.54645
	b2*	-0.03541	0.0215
	K	273	0
ln P	a0*	-2159.8567	629.62864
	a1*	-294.99601	162.47123
	a2*	15.22036	7.34837
	a3*	-0.22164	0.12131
	a4*	0.00374	0.00232
--	a5*	-2.27363E-	1.56546E-5
	b0*	10.50414	2.17915
	b1*	0.89928	0.54645
	b2*	-0.03541	0.0215
	K	298	0

Fig. S14 The C_2H_2 fit isotherms of **HUST-5** at 273 K and 298 K by virial equation.

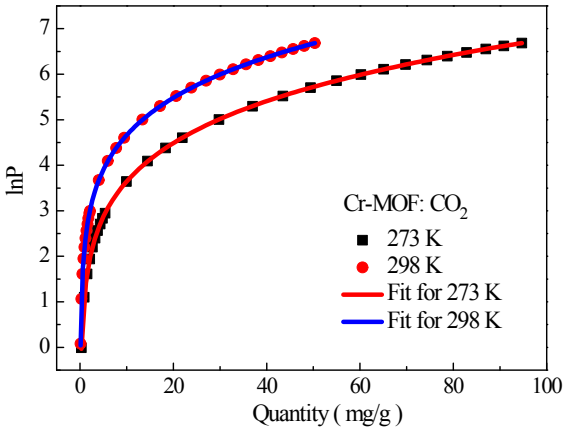

Model	Qst (User)		
Equation	y=ln(x)+1/K*(a0+a1*x+a2*x^2+a3*x^3 +a4*x^4+a5*x^5)+(b0+b1*x+ b2*x^2)		
Reduced Chi-Sqr			5.13264E-5
Adj. R-Square			0.99999
		Value	Standard Err
Quantity	a0*	-3406.3843	11.85923
	a1*	10.03323	1.56801
	a2*	-0.0734	0.0376
	a3*	-4.97527E-	5.74767E-4
	a4*	9.63397E-	7.07468E-6
--	a5*	-4.65536E-	3.07959E-8
	b0*	13.64576	0.04091
	b1*	-0.01852	0.00533
	b2*	1.84652E-	1.08637E-4
	K	273	0
ln P	a0*	-3406.3843	11.85923
	a1*	10.03323	1.56801
	a2*	-0.0734	0.0376
	a3*	-4.97527E-	5.74767E-4
	a4*	9.63397E-	7.07468E-6
--	a5*	-4.65536E-	3.07959E-8
	b0*	13.64576	0.04091
	b1*	-0.01852	0.00533
	b2*	1.84652E-	1.08637E-4
	K	298	0

Fig. S15 The CO_2 fit isotherms of HUST-6 at 273 K and 298 K by virial equation.

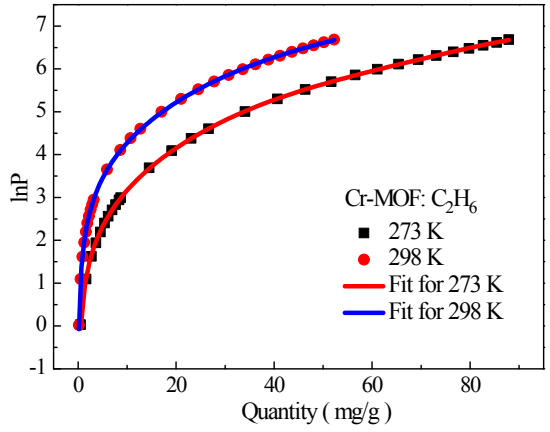

Model	Qst (User)		
Equation	y=ln(x)+1/K*(a0+a1*x+a2*x^2+a3*x^3 +a4*x^4+a5*x^5)+(b0+b1*x+ b2*x^2)		
Reduced Chi-Sqr			6.02475E-4
Adj. R-Square			0.99984
		Value	Standard Err
Quantity	a0*	-3731.819	46.78094
	a1*	11.8546	5.4047
	a2*	0.15999	0.12322
	a3*	-0.00617	0.00239
	a4*	7.71808E-	3.16795E-5
--	a5*	-3.23501E	1.48622E-7
	b0*	14.24962	0.16046
	b1*	-0.01836	0.01841
	b2*	-5.46887E	3.54969E-4
	K	273	0
ln P	a0*	-3731.819	46.78094
	a1*	11.8546	5.4047
	a2*	0.15999	0.12322
	a3*	-0.00617	0.00239
	a4*	7.71808E-	3.16795E-5
--	a5*	-3.23501E	1.48622E-7
	b0*	14.24962	0.16046
	b1*	-0.01836	0.01841
	b2*	-5.46887E	3.54969E-4
	K	298	0

Fig. S16 The C_2H_6 fit isotherms of HUST-6 at 273 K and 298 K by virial equation.

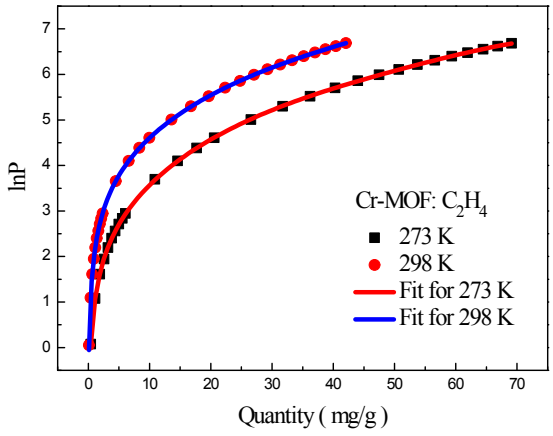

Model		Qst (User)	
Equation		y=ln(x)+1/K*(a0+a1*x+a2*x^2+a3*x^3 +a4*x^4+a5*x^5)+(b0+b1*x+ b2*x^2)	
Reduced Chi-Sqr			3.64278E-4
Adj. R-Square			0.99991
		Value	Standard Err
Quantity	a0*	-3637.0611	35.13048
	a1*	28.2515	5.14649
	a2*	-0.13061	0.14983
	a3*	-0.00851	0.00388
	a4*	1.44723E-	6.5272E-5
--	a5*	-8.1949E-7	3.88752E-7
	b0*	14.25163	0.12074
	b1*	-0.07211	0.01754
	b2*	9.55144E-	4.23718E-4
	K	273	0
ln P	a0*	-3637.0611	35.13048
	a1*	28.2515	5.14649
	a2*	-0.13061	0.14983
	a3*	-0.00851	0.00388
	a4*	1.44723E-	6.5272E-5
--	a5*	-8.1949E-7	3.88752E-7
	b0*	14.25163	0.12074
	b1*	-0.07211	0.01754
	b2*	9.55144E-	4.23718E-4
	K	298	0

Fig. S17 The C_2H_4 fit isotherms of HUST-6 at 273 K and 298 K by virial equation.

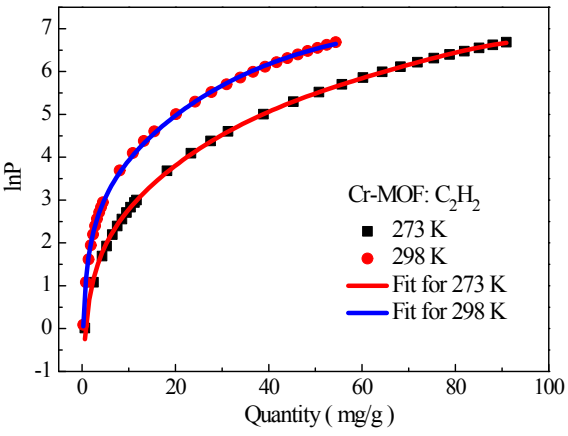

Model		Qst (User)	
Equation		y=ln(x)+1/K*(a0+a1*x+a2*x^2+a3*x^3 +a4*x^4+a5*x^5)+(b0+b1*x+ b2*x^2)	
Reduced Chi-Sqr			0.00245
Adj. R-Square			0.99936
		Value	Standard Err
Quantity	a0*	-3525.4101	104.86919
	a1*	-27.88162	10.88968
	a2*	0.87027	0.23159
	a3*	-0.00927	0.00435
	a4*	1.05326E-	5.56546E-5
--	a5*	-4.27189E-	2.52202E-7
	b0*	13.12882	0.35871
	b1*	0.12033	0.03713
	b2*	-0.00208	6.71825E-4
	K	273	0
ln P	a0*	-3525.4101	104.86919
	a1*	-27.88162	10.88968
	a2*	0.87027	0.23159
	a3*	-0.00927	0.00435
	a4*	1.05326E-	5.56546E-5
--	a5*	-4.27189E-	2.52202E-7
	b0*	13.12882	0.35871
	b1*	0.12033	0.03713
	b2*	-0.00208	6.71825E-4
	K	298	0

Fig. S18 The C_2H_2 fit isotherms of HUST-6 at 273 K and 298 K by virial equation.

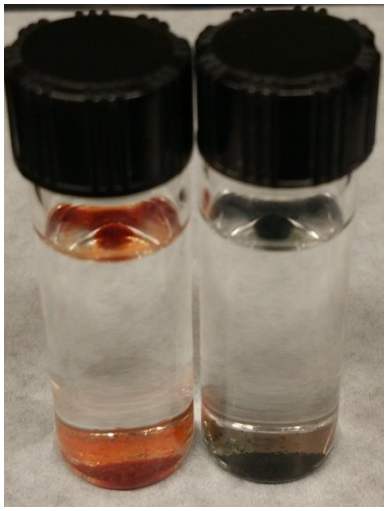

Figure S19. Photo images of HUST-5 and HUST-6

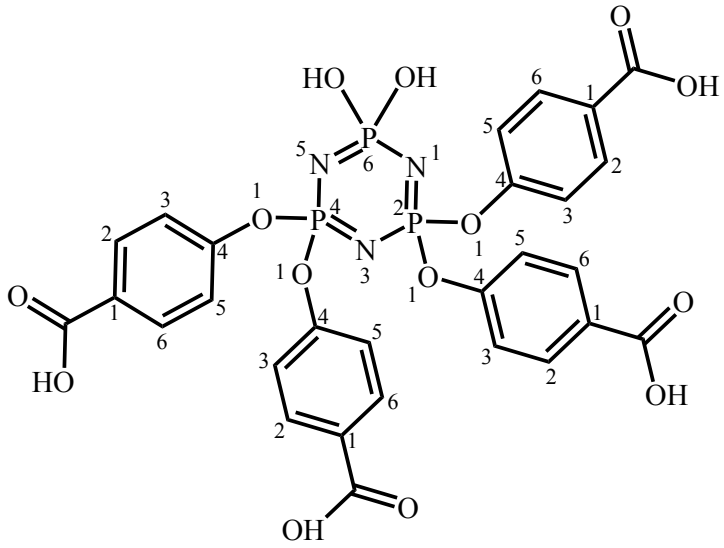

Scheme S1. The simplified ligand in the theoretical calculation model, named as 4,4',4",4"'-((6,6-dihydroxy-1,3,5,2l5,4l5,6l5-triazatriphosphinine-2,2,4,4-tetrayl)tetrakis(oxy))tetrabenzoic acid (L2)

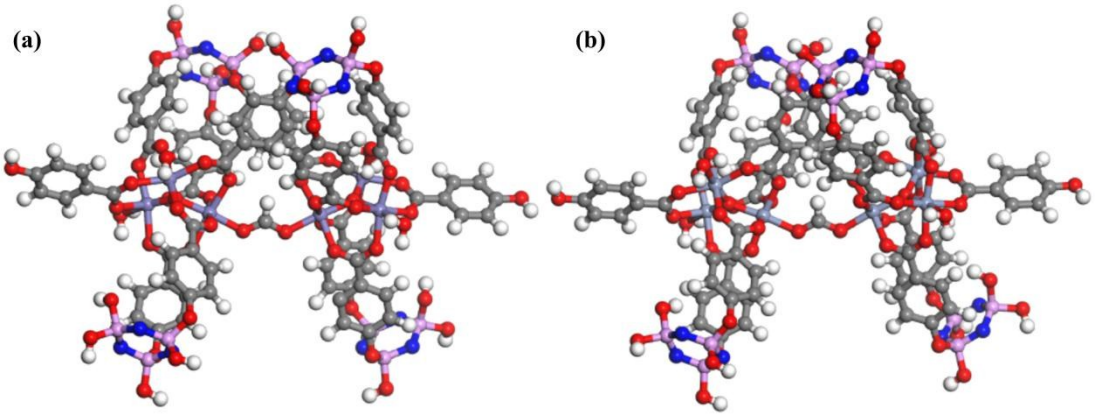

Figure S20. relaxed structure of $(M_3O)_2(H_2O)_4(HCOO)(L2)_4$ (M= Fe(a), Cr(b))

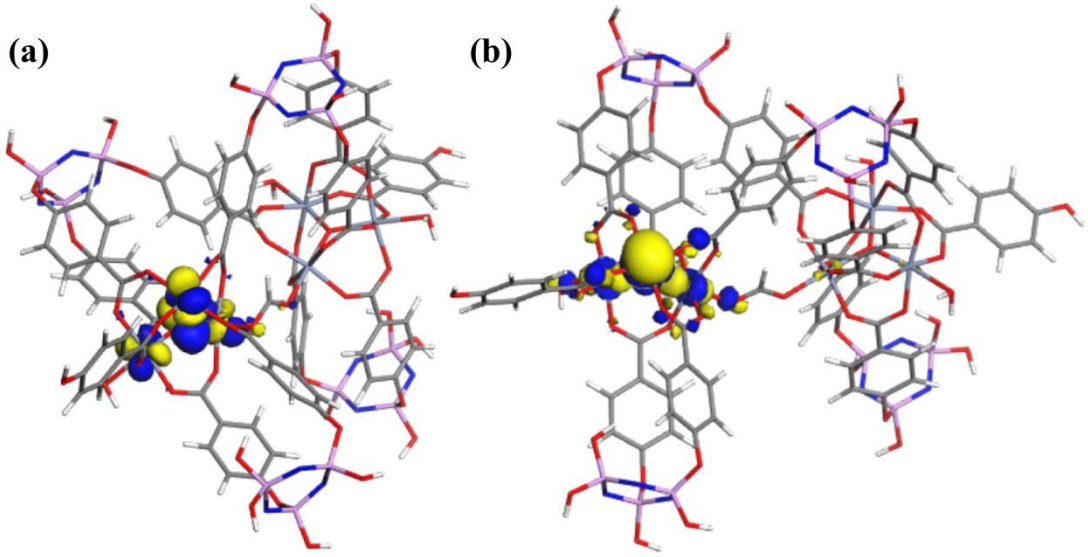

Figure S21. HOMO (a) and LUMO(b) of hexa-nuclear chromium cluster.

Table S4. Summary of the adsorption uptakes, selectivity and heat of adsorption data for C_2H_2 and C_2H_4 in various MOFs.

	MOF-74-Fe[7]	UTSA-100a[8]	NOTT-300[10]	SIFSIX-1-Cu[9]	NKMOF-1-Ni[11]	NbU-1[12]	HUST-6
BET($m^2\ g^{-1}$)	1350	970	1370	1178	280	368	645.3
C_2H_2 uptake ($cm^3\ g^{-1}$)	152.3	95.6	142.0	190.4	61	81.5	78.3
C_2H_4 uptake ($cm^3\ g^{-1}$)	136.6	37.2	95.9	92.1	47.3	46.4	53.2
Qst (C_2H_2 kJ mol^{-1})	47	22	32	30/37	60.3	38.3	31.1
Qst (C_2H_4 kJ mol^{-1})	45	-	16	23.5	44.9	37.9	30.2
Selectivity for C_2H_2/C_2H_4 50/50 mixture	1.87	10.72	2.3	8.37	-	5.9	3.8
τ_{break}[14]	71.52	52.04	56.14	92.31	-	319.24	132.25

C_2H_x uptake data: at 273K and 1.0 bar (the temperature for MOF-74-Fe is 318 K, for NOTT-300 is 293 K). The selectivity data: calculated by IAST for an equimolar mixture at 1.0 bar and 298K. Dimensionless breakthrough time (τ_{break}) : Breakthrough calculations for separation of C_2H_2/C_2H_4 mixture (50/50) at 293K for HUST-6. The data for MOF-74-Fe is at a temperature of 318 K. The data for **UTSA-100a** and ***SIFSIX-2-Cu-i*** is at a temperature of 298 K.

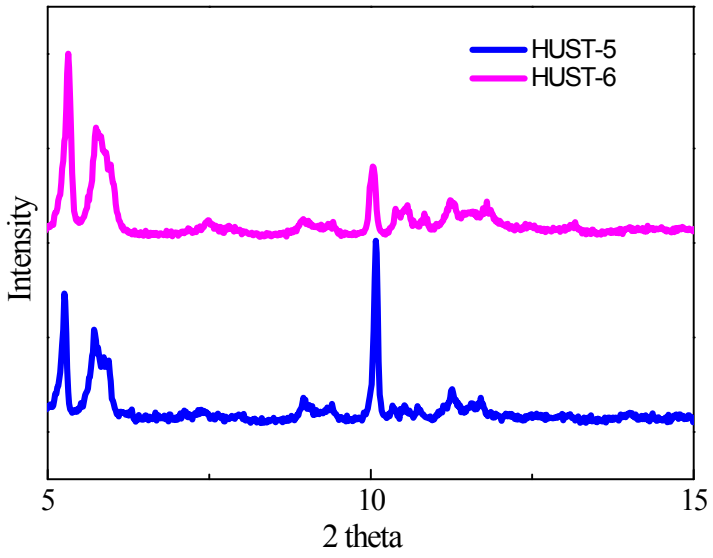

Figure S22. The enlarged PXRD patterns of HUT-5 and HUS-6

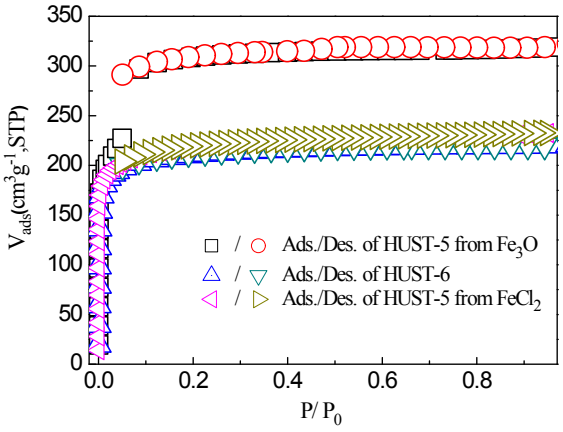

Figure S23. N_2 sorption isotherms for activated HUST-5 derived from Fe_3O cluster, HUST-6 and HUST-5 derived from $FeCl_2$ cluster at 77K after vacuum-drying at 150 °C overnight.

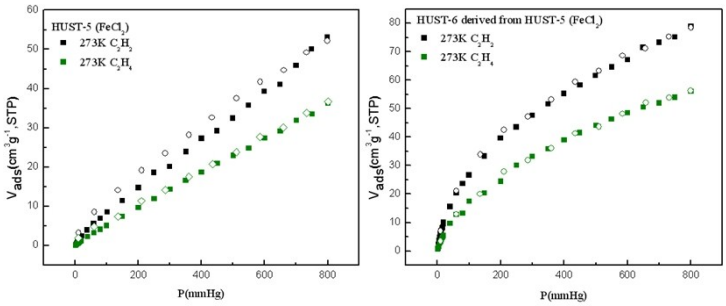

Figure S24. C_2H_4 and C_2H_2 sorption isotherms for HUST-5 (Fe-Cl_2, left) and HUST-6 (Fe-Cl_2, right)

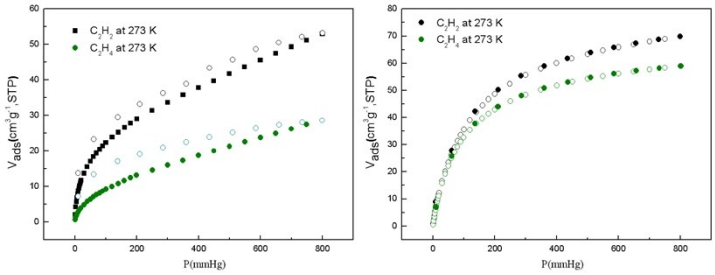

Figure S25. C_2H_4 and C_2H_2 sorption isotherms for MIL-100 (Fe, left) and MIL-100 (Cr, right)

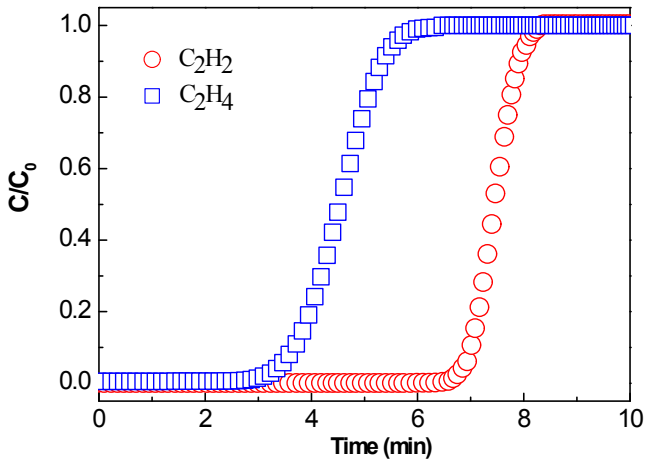

Figure S26. Breakthrough curves for C_2H_2/C_2H_4 separations (10/90) (b) for MIL-100(Cr).

References:

S1. C. T. Dziobkowski, J. T. Wrobleski, and D. B. Brown. Inorg. Chem. 1981, 20, 679-684.

S2. B. Li, X. Dai, X. Meng, T. Zhang, C. Liua and K. Yu. Dalton Trans., 2013, 42, 2588–2593.

S3. (a)B. Delley, J. Chem. Phys., 1990, 92, 508; (b)B. Delley, J. Chem. Phys., 1991, 94, 7245; (c) B. Delley, J. Chem. Phys., 2000, 113, 7756.

S4. H. J. Monkhorst and J. D. Pack, Phys. Rev. B, 1976, 13, 5188.

S5. J. P. Perdew, K. Burke and M. Ernzerhof, Phys. Rev. Lett., 1996, 77, 3865.

S6. M. Dolg, U. Wedig, H. Stoll, Preuss, H. J. Chem. Phys., 1987, 86, 866.

S7. E. D. Bloch, W. L. Queen, R. Krishna, J. M. Zadrozny, C. M. Brown, J. R. Long, Science, 2012, 335, 1606-1610.

S8. T. L. Hu, H. Wang, B. Li, R. Krishna, H. Wu, W. Zhou, Y. Zhao, Y. Han, X. Wang, W. Zhu, Z. Yao, S. Xiang, B. Chen, Nat. Commun., 2015, 6, 7328

S9. X. Cui, K. Chen, H. Xing, M. J. Zaworotko, B. Chen, Science, 2016, 353, 141-144.

S10. S. Yang, A. J. Ramirez-Cuesta, R. Newby, V. Garcia-Sakai, P. Manuel, S. K. Callear, S. I. Campbell, C. C. Tang, M. Schröder, Supramolecular binding and separation of hydrocarbons within a functionalized porous metal-organic framework. Nat. Chem. 2014, 7, 121–129.

S11. Y.-L. Peng, T. Pham, P. Li, T. Wang, Y. Chen, K.-J. Chen, K. A. Forrest, B. Space, P. Cheng, M. J. Zaworotko, Z. Zhang, Angew. Chem., Int. Ed., 2018, 57, 10971–10975.

S12. J. Li, L. Jiang, S. Chen, A. Kirchon, B. Li, Y. Li, H. C. Zhou. J. Am. Chem. Soc. 2019, 141, 3807−3811.